Click Here for Full Article

Coupled modelling of glacier and streamflow response to future climate scenarios

K. Stahl,[1,2] R. D. Moore,[1] J. M. Shea,[1] D. Hutchinson,[3] and A. J. Cannon[3]

Received 7 February 2007; revised 22 August 2007; accepted 27 December 2007; published 16 February 2008.

[1] This study investigated the sensitivity of streamflow to changes in climate and glacier cover for the Bridge River basin, British Columbia, using a semi-distributed conceptual hydrological model coupled with a glacier response model. Mass balance data were used to constrain model parameters. Climate scenarios included a continuation of the current climate and two transient GCM scenarios with greenhouse gas forcing. Modelled glacier mass balance was used to re-scale the glacier every decade using a volume-area scaling relation. Glacier area and summer streamflow declined strongly even under the steady-climate scenario, with the glacier retreating to a new equilibrium within 100 years. For the warming scenarios, glacier retreat continued with no evidence of reaching a new equilibrium. Uncertainty in parameters governing glacier melt produced uncertainty in future glacier retreat and streamflow response. Where mass balance information is not available to assist with calibration, model-generated future scenarios will be subject to significant uncertainty.

Citation: Stahl, K., R. D. Moore, J. M. Shea, D. Hutchinson, and A. J. Cannon (2008), Coupled modelling of glacier and streamflow response to future climate scenarios, *Water Resour. Res.*, *44*, W02422, doi:10.1029/2007WR005956.

1. Introduction

[2] Glaciers influence streamflow variability on a range of time scales [*Fountain and Tangborn*, 1985]. In particular, glacier melt can maintain streamflow during the summer dry season when rivers with non-glacierized basins experience extreme low flow. Glaciers also appear to regulate summer water temperatures in downstream rivers [*Brown et al.*, 2005; *Moore*, 2006] and thus maintain high-quality habitat for cold-water species such as salmonids. There is increasing concern that climatic warming will cause accelerated glacier retreat, in turn resulting in decreased summer streamflow [*Barnett et al.*, 2005]. However, changes in glacier mass balance may not necessarily produce an immediate decrease in streamflow. Following the initial shift from a positive or neutral mass balance to a negative balance, melt water generation may increase due to the earlier disappearance of high-albedo snow and the exposure of lower-albedo firn and/or ice, as well as the effects of increased energy inputs [*Braun and Escher-Vetter*, 1996; *Singh and Kumar*, 1997]. Indeed, recent warming trends in southwestern Yukon-northwestern British Columbia have been accompanied by positive streamflow trends in glacier-fed catchments [*Fleming and Clarke*, 2003]. Similarly, streamflow in glacier-fed Himalayan rivers has been increasing [*WWF*, 2005]. However, an initial increase in glacier runoff cannot be sustained because, in the longer term, glacier recession will decrease glacier area sufficiently to reduce meltwater volumes. While streamflow in glacierized rivers in Switzerland increased during the summer heatwave of 2003 [*Zappa and Kan*, 2007], a modelling experiment in the glaciated Goldbergkees catchment in Austria by *Koboltschnik et al.* [2007] revealed that if the 2003 summer weather had occurred in 1979, when the glacier area was larger (71% vs 52% of catchment), annual discharge would have been 12% higher and daily discharge up to 35% higher than observed in 2003.

[3] As in many other mountain regions worldwide, most glaciers in British Columbia are currently retreating [*Oerlemans*, 2005; *Moore and Demuth*, 2001; *Schiefer et al.*, 2007]. Because glaciers are such an important source of freshwater, current and future retreat raises concerns over the sustainability of water supplies and fish habitat. *Stahl and Moore* [2006] examined trends in August streamflow for 236 hydrometric stations in British Columbia that capture a range of glacier cover extents. Glacier-fed streams exhibited significant negative trends, both with and without corrections for interannual variability in climatic forcing. These results suggest that in most regions of BC, the phase of initially increased melt contribution has passed. Other mountainous regions in the world show similar patterns [*Collins*, 2006] and the issue of potential effects of future changes in climate regimes and glacier cover on hydrology has received considerable attention.

[4] Precipitation-runoff models have been used to estimate the effect of climate change on streamflow in glacier-fed basins. However many of these studies did not adjust the glacier cover to account for glacier response to the imposed climatic changes [e.g., *Moore*, 1992; *Singh and Bengtsson*, 2005], limiting the time scale over which the results could apply. *Hagg et al.* [2006] examined the effect of an assumed reduction in glacier area in central Asia, but did not model the transient streamflow response associated with changing glacier area. *Horton et al.* [2006] updated the glacier area

[1]Department of Geography, The University of British Columbia, Vancouver, B.C., Canada.
[2]Now at Department of Geosciences, University of Oslo, Oslo, Norway.
[3]Environment Canada, Vancouver, B.C., Canada.

Copyright 2008 by the American Geophysical Union.
0043-1397/08/2007WR005956$09.00

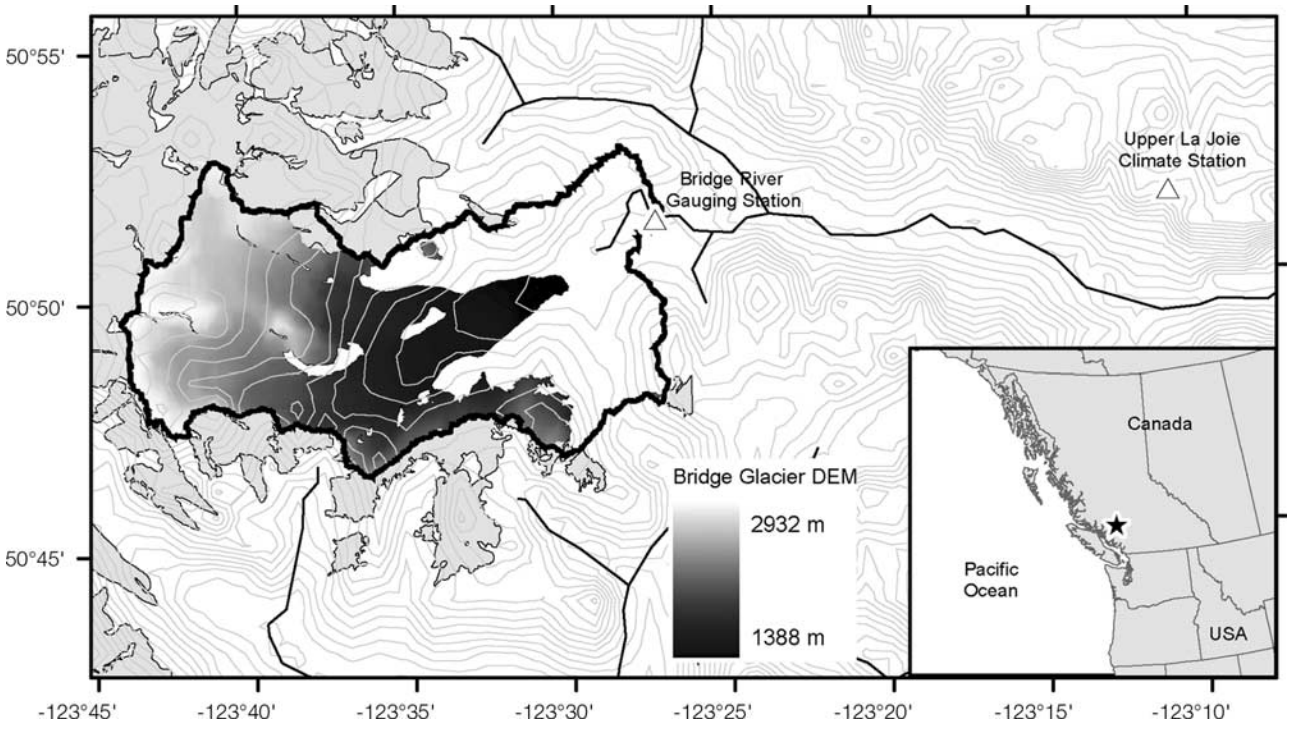

Figure 1. Map of Bridge River basin with DEM of Bridge Glacier.

for simulation of future conditions assuming a constant accumulation-area ratio, but also did not address transient responses. Only the study by *Rees and Collins* [2006] appears to have considered the transient response associated with glacier retreat. They assumed a simplified glacier geometry and removed elevation bands as ice thickness depleted.

[5] Glaciologists have used two main approaches to modelling the transient response of glaciers to climate changes. The most physically rigorous is through dynamical modelling [e.g., *Oerlemans et al.*, 1998]. However, this approach is computationally intensive and not well suited for extensive regions with sparse climate data and little to no information about past glacier dynamics. The alternative approach is to use a specified relation between glacier volume and glacier area, which was originally derived empirically [*Chen and Ohmura*, 1990], but which has since been derived through considerations of the physics of glacier flow [*Bahr et al.*, 1997]. This approach involves using the volume-area scaling relation to estimate future changes in glacier area that would be associated with changes in glacier volume based on simulated future mass balance. While this approach has been used in many glaciological studies [e.g., *van de Wal and Wild*, 2001; *Radic and Hock*, 2006], to our knowledge it has not yet been incorporated into a hydrological simulation.

[6] The objective of this study was to develop and apply a methodology for estimating changes in streamflow associated with the coupled effects of climatic change and associated glacier response, with a specific focus on transient responses. The approach combines conceptual models of catchment hydrology and glacier mass balance with a model of glacier area evolution based on volume-area scaling. After calibration and validation, the combined model is driven with three different sets of climate scenarios: a scenario created with a weather generator that assumes a continuation of the climate of the last decades; and two scenarios downscaled from a GCM based on climate response to increased greenhouse-gas concentrations. The approach will allow comparison with the aforementioned empirical trends and provide a basis for assessing the hydrologic effects of future glacier changes.

2. Study Area and Data

[7] This study focused on the Bridge River catchment, located in the Southern Chilcotin Mountains, a transition zone from wet coastal mountains to dry interior climate in southern British Columbia, Canada (Figure 1). The Bridge River Complex is the third largest hydropower development operated by BC Hydro. Hence, any future changes in streamflow are of considerable socio-economic concern.

[8] Basin boundary and land cover information were derived by Environment Canada from the base thematic map (BTM) of British Columbia, which is based on Landsat Imagery from the early 1990s. The basin drains an area of 152.4 km^2, of which the BTM glacier cover is 61.8% (92 km^2), and spans an elevation range from 1400 m.a.s.l. to 2900 m.a.s.l. Hydrometric data are available since the early 1980s from HYDAT, the database of the Water Survey of Canada. Average annual runoff during the period of record was ca. 2600 mm/year. Climate data are available from a high elevation (1829 m.a.s.l.) weather station ("Upper La Joie"), which has been operated by BC Hydro since 1985 and provides the climate input routinely used in their inflow forecasting models. Daily temperature, precipitation and discharge data of sufficient quality and completeness for application of a hydrological model are available for the period 1985 to 2004.

[9] Mass balance surveys on Bridge Glacier were carried out from 1977 to 1985 [*Mokievsky-Zubok et al.*, 1985;

Dyurgerov, 2002]. Unfortunately, this period is prior to the period chosen for the hydrological modelling and hence cannot be used directly for validation of the glacier model. However, the total net mass balance record at Bridge Glacier correlates well ($r^2 = 0.83$) with that of Place Glacier [*Dyurgerov*, 2002], located 80 km to the south-east. For the purpose of this study, Bridge Glacier mass balance values were reconstructed at 100 m intervals (1450 – 2850 m) using simple linear regressions with the mass balance record at Place Glacier (1850 – 2550 m) at a similar or closest available elevation. Winter and summer mass balance reconstructions were performed separately, and net annual mass balances for each elevation band at Bridge Glacier were calculated as the sum of reconstructed winter and summer balances. The strength of the individual regressions varied from $R^2 = 0.41–0.86$ (summer balance) to $R^2 = 0.24 – 0.87$ (winter balance), reflecting the broad regional coherence of glacier mass balance.

3. Methods

3.1. The HBV-EC Model

[10] Streamflow was modelled using the HBV-EC semi-distributed conceptual hydrological model [*Hamilton et al.*, 2000], which is based on the Swedish HBV model [*Lindström et al.*, 1997]. An earlier version was applied with reasonable success to the 17% glacier-covered Lillooet River catchment, immediately south of Bridge River [*Moore*, 1993]. The current HBV-EC model was integrated into the EnSim™ modelling environment [*Canadian Hydraulics Centre*, 2006] to leverage data pre- and post-processing and model visualization capabilities. The model allows for discretization of the watershed into climate zones to account for horizontal gradients in basin climatology. Within each climate zone, the HBV-EC model uses the Grouped Response Unit (GRU) concept to group DEM/GIS grid cells into bins having similar land cover, elevation, slope, and aspect, in order to maintain computational efficiency. In this application, Bridge River Basin, which has four types of land cover (glacier, non-forest land, forest, and lake), was discretized into 14 elevation bands of 100 vertical metres, two aspects (north/south) and two slope classes.

[11] The model was run using a daily time step, consistent with the resolution of climate data. Correction factors for snowfall (*SFCF*) and rainfall (*RFCF*) adjust recorded precipitation to correct for gauge undercatch as well as bias associated with differences in precipitation between the basin and the climate station. Input climate data were adjusted for elevation using a lapse rate for temperature (*TLAPSE*) and separate gradients for precipitation below (*PGRADL*) and above (*PGRADH*) a threshold elevation (*EMID*). Both temperature lapse rates and precipitation gradients do not vary seasonally. The dominant phase of precipitation (rain vs. snow) occurring within an elevation band is determined by the threshold temperature (*TT*) and mixed-phase precipitation can occur within a temperature interval (*TTI*) around the threshold temperature. In forested areas, interception loss is treated as a constant fraction of precipitation, with separate fractions applied to rain and snowfall.

[12] Snow melt is computed using a temperature index approach based mainly on HBV algorithms. The parameters include a threshold temperature for melt (*TM*) and a base melt factor (C_0) that varies sinusoidally from a minimum value ($C_{\min}$) on the winter solstice to a maximum value on the summer solstice ($C_{\min} + DC$). The melt factor for open, flat areas is adjusted for slope (s) and aspect (a) following a simple trigonometric function:

$$C'(t) = C_0(t) \cdot (1 - AM \cdot \sin(s) \cdot \cos(a)) \quad (1)$$

where *AM* is a calibration parameter. In forested areas, the melt factor is further multiplied by *MRF* (ranging between 0 and 1) to account for the shading and sheltering effects of forest cover on melt rates. The melt factor for glacier GRUs is enhanced by the coefficient *MRG* once seasonal snowpack has ablated to reflect a reduction in surface albedo associated with a bare ice cover.

[13] Refreezing of liquid water can occur when air temperature is below the melt threshold, at a rate governed by the parameter *CRFR*. Soil evaporation, soil moisture storage and drainage are modelled according to established HBV algorithms [*Hamilton et al.*, 2000].

[14] Runoff routing is computed separately for glacierized and non-glacierized GRUs. For non-glacierized GRU's, water draining from the soil reservoirs enters a common set of lumped reservoirs, representing "fast" and "slow" drainage, as is common in HBV implementations [*Hamilton et al.*, 2000]. In contrast, each glacier GRU has a separate reservoir for runoff routing, outflow from which is calculated as:

$$Q_g(t,g) = KG(t,g) \cdot S(t,g) \quad (2)$$

where $S(t, g)$ is the liquid water stored in the reservoir at time t for glacier GRU g (mm) and $KG(t, g)$ is a time-varying outflow coefficient, parameterized as a function of snowpack water equivalent:

$$KG(t,g) = KG_{\min} + dKG \cdot \exp[-AG \cdot SWE(t,g)] \quad (3)$$

where $KG(t, g)$ is the outflow coefficient for time t and glacier GRU g (time^{-1}); $KG_{\min}$ is a minimum value, representing conditions with deep snow and poorly developed sub-, en- and supra-glacial drainage systems (time^{-1}); $KG_{\min} + dKG$ is the maximum outflow coefficient, representing late-summer conditions with bare ice and a well developed glacial drainage system; *AG* is a calibration parameter (mm^{-1}); and $SWE(t, g)$ is the snowpack water equivalent for time t and glacier GRU g (mm). The streamflow at the basin outlet is the sum of the outflow from the fast reservoir (Q_1), the slow reservoir (Q_2) and the glacier reservoirs ($Q_g(g)$).

3.2. Glacier Mass Balance Calculation

[15] The glacier module allows the calculation of annual glacier mass balances by GRU from the modelled time series of snow water equivalent (*SWE*) and ice melt (M_{ice}). By analogy with the stratigraphic method for mass balance computation [*Østrem and Brugman*, 1991], the winter balance for a given year and GRU, $b_w(t, g)$, is the maximum daily value of $SWE(t, g)$ for that year. The summer balance

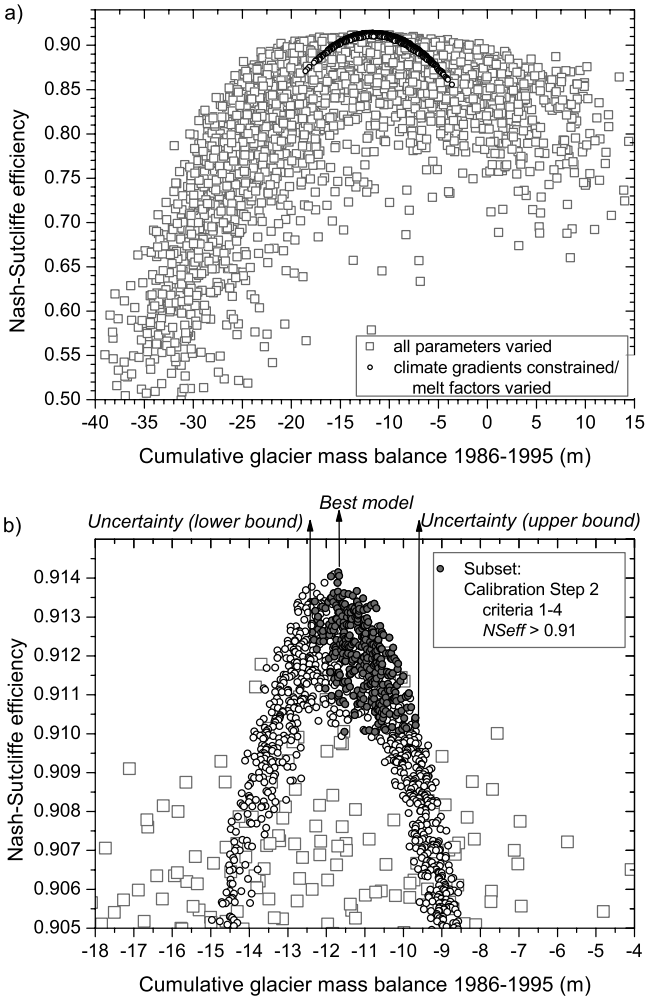

Figure 2. (a) Cumulative glacier mass balance versus NS efficiency for 4000 model runs with random variation of all parameters and 2000 model runs with constrained climate input and variation of snow and ice melt parameters, (b) subset meeting calibration criteria.

(b_s) depends on whether or not all of the snow melts off the glacier, with

$$b_s(g) = \min[SWE(t,g)] - \max[SWE(t,g)] \quad \text{if } \min[SWE(t,g)] > 0 \tag{4}$$

and

$$b_s(g) = -\left[\max[SWE(t,g)] + \sum M_{ice}(g)\right] \quad \text{if } \min[SWE(t,g)] = 0 \tag{5}$$

where $\Sigma M_{ice}(g)$ is the cumulative ice melt for the year, up to the date of the onset of continuous snow cover over the GRU.

[16] The net balance ($b_n(g)$) for each GRU is then

$$b_n(g) = b_w(g) + b_s(g) \tag{6}$$

and the total mass balance MB (as a volume) for the glaciers in the basins in a given year can then be computed as

$$MB = \sum_g \left(A_g \cdot b_n(g)\right) \tag{7}$$

where A is area and the subscript g refers to each glacier GRU.

3.3. Model Calibration and Validation

[17] Modelling highly seasonal hydrographs in snow and glacier dominated, data sparse catchments commonly has two major challenges: finding suitable calibration criteria or objective functions, and potential compensation of errors in calibrated climate gradients by snow and ice melt parameters. Nash-Suttcliffe efficiencies (NS_{eff}) [*Nash and Sutcliffe*, 1970] in seasonal hydrographs are commonly high, but do not necessarily provide a suitable objective function. In the present case, a benchmark model constructed from mean day-of-the-year values according to *Schaefli and Gupta* [2007] already had a NS_{eff} of 0.88. An initial global parameter search (4000 model runs) revealed many parameter combinations exceeding this benchmark with different combinations of climate gradients and snow and ice melt parameters. These models resulted in different cumulative glacier mass balances (Figure 2a).

[18] *Schaefli et al.* [2005] previously demonstrated the benefit of using mass balance data in the calibration process. To calibrate the model for the period 1986–1995 we therefore employed a three-step multi-model, multi-criteria approach that made use of a variety of objective functions for streamflow comparison, as well as the six years of reconstructed mass balance data. The objective of the approach was to determine the best model for streamflow while realistically reproducing glacier mass balances. First, the precipitation correction factor was adjusted to fit the reconstructed winter mass balances at the corresponding elevation of the climate station (located outside the basin). Then, in each of the calibration steps, 2000 model runs were performed with random combinations of the most sensitive parameters. The parameters were chosen according to an optimum in the respective objective function and/or by applying further limiting criteria (Table 1). The model was validated for the period 1996–2004 using observed streamflow.

3.4. Simulating Glacier Retreat and Advance

[19] Glacier advance or retreat was simulated by combining the modelled mass balance with the volume-area scaling relation introduced by *Chen and Ohmura* [1990], which was based on measured geometries of alpine glaciers around the world:

$$V = \mathrm{b} \cdot A^{1.36} \tag{8}$$

$$A = (V/\mathrm{b})^{0.735} \tag{9}$$

where V is the glacier volume ($m \cdot km^2$), b = 28.5, and A is the glacier area (km^2). The physical basis of the relation was confirmed by *Bahr et al.* [1997], who also updated the empirical relation with additional data. Bridge Glacier lies

Table 1. Calibration Approach

Step	Parameters Varied	Criterion	Selection
Step 1	Climate gradients	1. MAE winter mass balance[a]	minimum
Step 2	Snow and glacier melt factors	1. Mean August streamflow	error < 5%
		2. Mean annual streamflow	error < 5%
		3. MAE summer mass balance[a]	<310 mm
		4. NS_{eff} (April–July)	>0.84
		5. NS_{eff}	best of above (best model) > 0.91 (uncertainty bounds)
Step 3	Routing parameters	1. Mean August streamflow	error < 5%
		2. NS_{eff} for log of streamflow	>0.8
		3. NS_{eff}	>0.915

[a]Mean absolute error between average reconstructed balance and simulated balance for 6 years and 9 elevation bands.

well within the range of glacier sizes that was used to derive the empirical volume area scaling relation. As no observations of the glacier depth exist for Bridge Glacier, the initial volume was derived from the current glacier area using equation (8). Each decade, the volume was updated by adding the computed change in volume, determined from the accumulated mass balance for the period (MB), and the new area (A_{new}) was computed using the scaling relation (equation (9)). The area that had to be removed or added was computed as

$$\Delta A = A_{new} - A_{old} \tag{10}$$

The removal (or addition) of glacier cover from the land use grid was simulated by an algorithm coded in IDL (Interactive Data Language). The glacier area change was first converted into the number of glacier pixels to be removed or added to the glacier. Glacier pixels were then removed or added along the edge of the glacier using a morphologic erosion or dilation operator, a common method in digital image processing to fill holes or remove islands and to expand/grow or reduce/shrink a binary image. The erosion or dilation is performed iteratively, removing one row of pixels in each of "n" passes, stopping when the total number of desired pixels has been removed or added. To reduce glacier area, glacier pixels along the glacier edge are first eroded from the lowest elevation band, then from the two lowest elevation bands, and so on up to the equilibrium line elevation (determined from the glacier mass balance model). This iterative removal mimics the stronger retreat of the glacier tongue and the effect can be increased by setting a higher number for the parameter "n" to erode proportionally more from lower elevations. Newly glacier-free areas were considered non-forest land for subsequent hydrologic simulations. To grow the glacier, the reverse procedure was performed. The glacier was allowed to grow into the area of its historical extent.

3.5. Climate Scenarios

[20] Three sets of future climate scenarios were established to model future glacier change and its impact on hydrology: S0, a continuation of the observed 1986–2004 climate over the next 200 years; and S1 and S2, representing climate downscaled from the SRES-B1 and A2 scenarios as calculated by the third version of the Canadian Centre for Climate Modelling and Analysis Coupled Global Climate Model (CGCM3) for the IPCC's Fourth Assessment Report (AR4). Among all GCMs that participated in the AR4 model intercomparison, the predictions by CGCM3 for the region rank in the middle for future temperature increase and at the upper end for precipitation increase [e.g., *Mote et al.*, 2005].

[21] The climate input variables for S0 were derived using the stochastic weather generator LARS-WG [http://www.rothamsted.bbsrc.ac.uk/mas-models/larswg.php]. LARS-WG generates weather data based on statistics of wet and dry spells, the distribution of rainfall amounts and temperature variability, which is conditioned on the wet and dry series [*Semenov et al.*, 1998].

[22] Scenarios S1 and S2 were derived using the TreeGen statistical downscaling model. TreeGen relates observed synoptic-scale atmospheric predictor fields to observed surface weather elements, and then, based on these relationships, generates realistic series of weather elements from GCM fields (details in Appendix A). Predictands in the TreeGen downscaling model were daily minimum temperature, maximum temperature, and precipitation amounts observed at the Upper La Joie weather station from 1985–2005. Gridded synoptic-scale mean sea-level pressure, surface air temperature, and surface precipitation data from the US National Centers for Environmental Prediction/National Center for Atmospheric Research (NCEP/NCAR) Reanalysis [*Kalnay et al.*, 1996] were used to define the historical synoptic map-types controlling daily weather conditions at Upper La Joie. Daily mean maps were obtained for the period 1961–2005 for a region covering western North America and the eastern Pacific Ocean (30°N–70°N; 160°W–110°W) on a grid subsampled to a

Table 2. Most Sensitive HBV Parameters

Model Component	Parameter	Description	Value
Climate	PFCF[a]	Precipitation correction factor	1.8
	PGRADL	Fractional precipitation increase with elevation (m^{-1})	0.0016
	PGRADH	Fractional precipitation increase above EMID (m^{-1})	0.0001
	EMID	Mid point elevation separating precipitation gradients (m)	2100
	TLAPSE	Temperature lapse rate (°C m^{-1})	0.006
Snow	AM	Influence of aspect/slope on melt factor	0.25
	TM	Threshold temperature for snowmelt (°C)	−0.69
	CMIN	Melt factor for winter solstice in open areas ($mm \cdot °C^{-1} \cdot day^{-1}$)	1.01
	DC	Increase of melt factor between winter and summer solstice ($mm \cdot °C^{-1} \cdot day^{-1}$)	2.08
Glacier	MRG	Ratio of melt of glacier ice to melt of seasonal snow	1.52

[a]Separate rainfall and snowfall records were not available for this climate station; hence, RFCF was applied to the total precipitation as a separate SFCF could not be used.

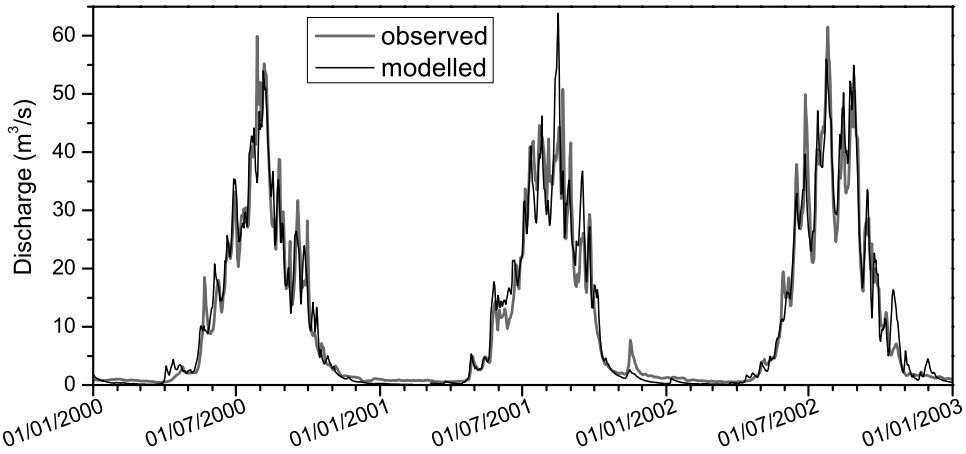

Figure 3. Observed and modelled hydrograph at gauging station Bridge River below Glacier.

spacing of 5° by 5°. Synoptic-scale fields matching those from the NCEP/NCAR Reanalysis were obtained from transient greenhouse gas plus aerosol runs of CGCM3 for simulated years 1961–2100.

[23] Forcing data for the scenarios S1 and S2 were from the IPCC SRES B1 and A2 scenarios, respectively. The SRES B1 scenario assumes low population growth, rapid changes towards a service and information economy, and the introduction of clean and resource-efficient technologies, whereas the A2 scenario assumes high population growth, an emphasis on regional economic development, and slower technological change. Equivalent CO_2 concentrations for the B1 scenario are projected to increase to 1.5 times year 2000 levels by 2100, while those for the A2 scenario are projected to increase to 2.5 times year 2000 levels by 2100.

[24] As LARS-WG and TreeGen both have stochastic components, ten realisations were computed for each scenario, creating an ensemble of ten members (M1, M2, ..., M10). Each member consists of a time series of daily temperature and precipitation. In the case of S0 these are 200 years long and are based on the statistics of the observed data from 1986 to 2005; in the case of S1 and S2 the time series represent the transient climate change as modelled by the GHG forced GCM scenarios. All scenarios were then used to drive the HBV-EC model with the glacier being re-scaled at the end of every decade based on the decade's cumulative mass balance. The effect of glacier re-scaling on streamflow was tested by applying a scenario run S1a, which had the same climate input as in S1 but without application of glacier scaling throughout the scenario period. That is, S1a maintained the glacier at its current extent.

4. Results

4.1. Calibration and Validation of HBV-EC

[25] The calibration procedure successfully identified models that reproduce observed streamflow and reconstructed mass balances. While Step 2 of the calibration reduced the number of viable models, a considerable subset still met the criteria using a range of snow and ice melt parameters. Figure 2b shows that this subset of models results in cumulative net balances between −12.4 m and −9.7 m for the calibration period. Such differences will affect the simulations of future glacier change. Hence, besides the best model, we also used the models producing the upper and lower bound of mass balances to illustrate the uncertainty in future model simulations due to the choice of snow and ice melt factors. Model results with these parameter combinations are added to following numbers and graphs as an uncertainty range.

[26] The best model achieved an efficiency of NS_{eff} = 0.91 for the calibration period and NS_{eff} = 0.93 for the validation period. Values for the most sensitive model parameters (Table 2) are comparable to those found in other applications of HBV-based models in glacierized catchments [e.g. *Moore*, 1993].

[27] The calibrated model reproduces the interannual variation in snowmelt and the glacial hydrograph, but it systematically underestimates the (low) winter streamflow (Figure 3). The range of mass balances and their variation with elevation during the calibration period are reproduced correctly by the model (Figure 4), except for the modelled summer balance in the lowest elevation bands, which is lower than the summer balances reconstructed from Place Glacier. However, Place Glacier's lowest elevation is about 2000 m.a.s.l. Therefore, the mass balance reconstruction for Bridge Glacier's lower elevation bands had to be based on correlations with much higher elevation bands on Place Glacier and reconstructed values may, therefore, not be as reliable as for higher elevations. Mass balances in the higher elevation bands were represented well and the interannual variability of the mass balance for the entire glacier is particularly well reproduced from the beginning of the 1990s.

[28] The modelled cumulative net mass balance of the glaciers in Bridge River Basin for the calibration period was −11.8 m. The initial volume-area scaling for the period 1995–2004 resulted in a loss of glacier area of 7.67 km^2 from the initial 91.7 km^2 in the 1990s, for an updated area of 84.04 km^2 (Figure 5) with an uncertainty of +1.2 and −0.1 km^2. Modelled glacier change between 1995 and 2004 compares well with recent pictures from Bridge Glacier, though the north branch lost connection with the main glacier tongue during that period.

[29] As the downscaling was performed from the transient CGCM3 scenario for the period 1961 to 2100, downscaled climate variables for 1986–2004 scenario years

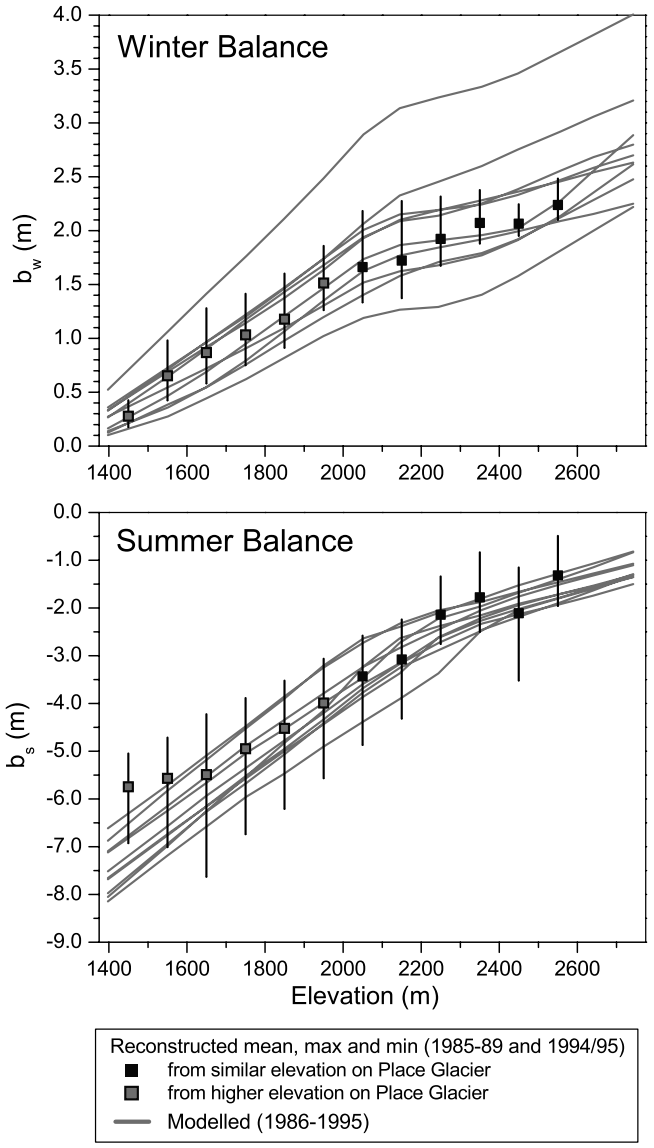

Figure 4. Reconstructed and modelled winter (upper panel) and summer (lower panel) mass balances for different elevation bands on Bridge Glacier.

could be compared with the observed climate and were used to run the HBV-EC model with the calibrated parameters. The average of the ten realisations shows slightly higher mean annual temperatures and slightly lower amounts of annual precipitation (Table 3). Seasonally, autumn was the most difficult to downscale, generally resulting in an overprediction of temperatures and an underprediction of precipitation in most realizations. However, observed averages and extreme values values lie well within the span of the ten realisations. Most important for the specific application in this study, however, is the validation of the downscaled climate in terms of the correct reproduction of mass balance and runoff variables, which show only small differences (Table 3).

4.2. Future Conditions Under Scenarios S0–S2

[30] While Scenario S0 maintains stationary climatic conditions, downscaled scenarios S1 and S2 mainly exhibit changes in temperature (Table 4). Annual temperatures for S2 increase particularly strongly after the middle of this century. A projected increase in winter precipitation is offset by a decrease in summer precipitation. Annual precipitation totals therefore remain relatively constant. Annual runoff decreases strongly for all scenarios and most strongly for S0, for which the decrease is entirely due to a decrease in ice melt. S1 and S2 are additionally influenced by seasonal changes in evapotransporation and snow accumulation and melt.

[31] The application of scenario S0 results in several more decades of negative mass balances, which causes further

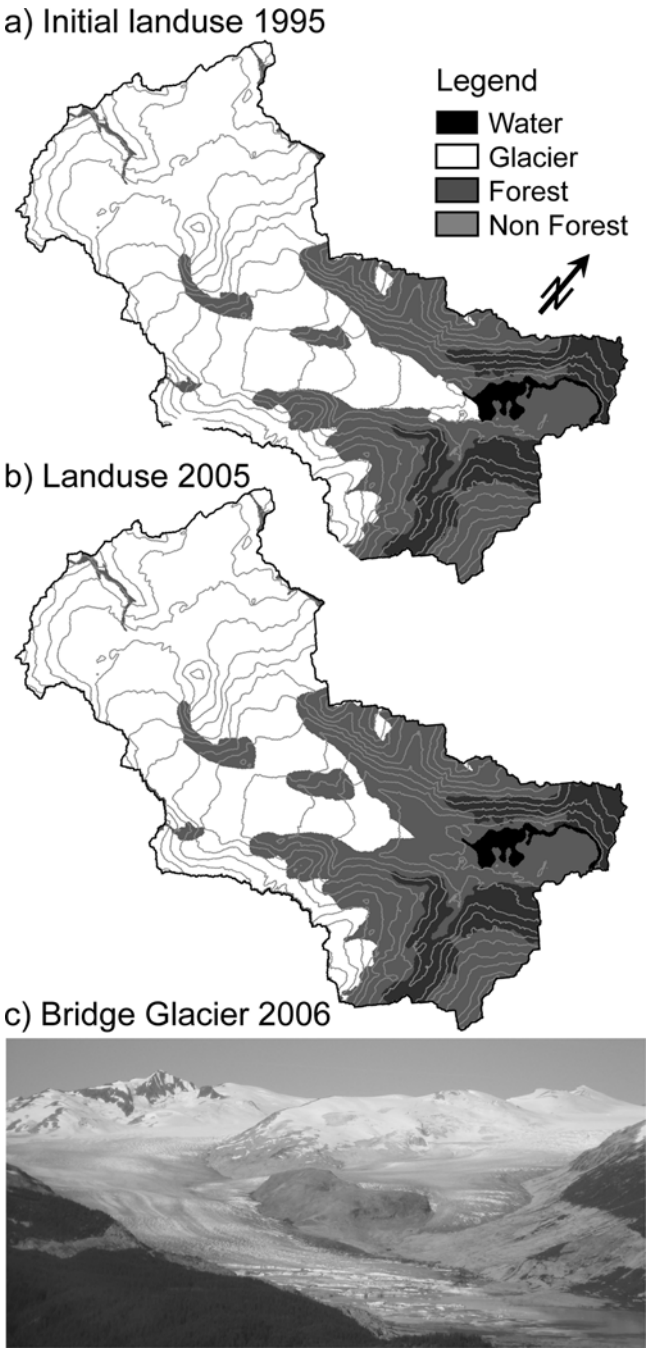

Figure 5. Land cover in Bridge basin: (a) initial glacier extent (b) re-scaled glacier after validation period in 2005 (c) photograph of Bridge Glacier in 2006.

Table 3. Mean Annual Variables Modeled for 1986–2004 (Range of 10 Realizations of Weather Sequences in Parentheses)

Climate Input	Basin Air Temperature, °C	Basin Precipitation, mm	Net Mass Balance, m	Runoff, mm
Observed	−0.19	2162	−1.24[a]	2680
S1	−0.03 (0.58)	2095 (394)	−1.16 (1.02)	2665 (417)
S2	−0.02 (0.50)	2023 (297)	−1.26 (0.62)	2646 (265)

[a]Mass balance for 1986–2004 is reconstructed, not observed directly.

retreat of the glacier over the next few decades. Mass balances then gradually approach zero and the glacier reaches an equilibrium with the current climate (where net mass balances fluctuate around zero) after ca. 90 years of simulation time (Figure 5). The glacier area decreases from the 84 km^2 in 2004 to 67 (±4) km^2, representing a loss of 20% of the present glacier area. Assuming no further climate change, the glacier coverage of the Bridge River basin could hence be expected to shrink from the original 62 % in the 1990s BTM map to ca. 43% at the end of the 21st century. In the new equilibrium, most of the two present glacier tongues disappear (Figure 6). The glacier shrinks even more rapidly in the downscaled climate change scenarios (Figures 6 and 7). Mass balances remain negative for S1 and strongly negative for S2 at the end of the century, with glacier area shrinking to 58.5 km^2 and 50 km^2, reducing basin glacier cover from the initial 62% to 38.5% and 33%, respectively.

[32] The glacier recession in all scenarios produces a decline in annual streamflow (Table 4). The streamflow decline is strongest in the summer months in the next few decades. For scenario S0 the initial drop of flow in August is followed by an asymptotic approach to an equilibrium flow of ca. 27 m^3/s with an uncertainty of +0.5 to −1 m^3/s, which is a reduction of 35% from the current 41 m^3/s (Figure 8). For S1 and S2, mean August streamflow will be even further reduced to about 25 m^3/s by 2095. The results for scenario S2 reflect the effect of a change in temperature increase by the middle of the century, when mass balances are even more negative and a relative increase in melt partially offsets the decrease in glacier area. The difference between streamflow trends for S0 and S1/S2 in other months show that increasing temperatures also result in a longer melt season with an earlier onset and longer duration of icemelt, which moderates the decrease of annual streamflow relative to S0 (Table 4), but increases glacier retreat.

Table 4. Change of Mean Annual Climate Input and Runoff Output Modeled for Future Time Slices Compared to 1986–2004 (Mean of 10 Realizations of Weather Sequences)

Time Slice	Climate Scenario	Basin Air Temperature, °C	Basin Precipitation, mm	Runoff, mm
2045–2055	S0	+0	+25	−554
	S1	+0.8	+17	−422
	S2	+0.9	−21	−338
2085–2095	S0	+0	−44	−699
	S1	+1.2	−16	−574
	S2	+2.4	−3	−450

[33] To illustrate the effect of glacier re-scaling on streamflow patterns, Figure 9 shows mean monthly streamflow for three time-slices for S1a and S1. With the same climate input, modelled streamflow increases considerably when the glacier area is kept constant, while it decreases considerably when the glacier area is reduced.

5. Discussion

[34] In general, the model fit to both streamflow and glacier mass balance is good and within the performance range of similar modelling applications in glacierized watersheds. The model tended to produce some systematic under- and overestimation of discharge, including an underestimation during winter. However, winter streamflow data are often influenced by ice cover and the record contains many periods of 'estimated' values, which may be higher than in reality. The error of about 5% in the annual flow is well within the range of common gauging errors. The climate station used in this study is located ca. 20 km from the basin outlet at a relatively high elevation of 1829 m. Though this station is fairly close to the basin, considering the remoteness of the area, the strong climatic gradients in the area required that some adjustments be made to the daily weather data. The value of *PFCF* = 1.8 reflects the drier climate at the station location compared to the glacier.

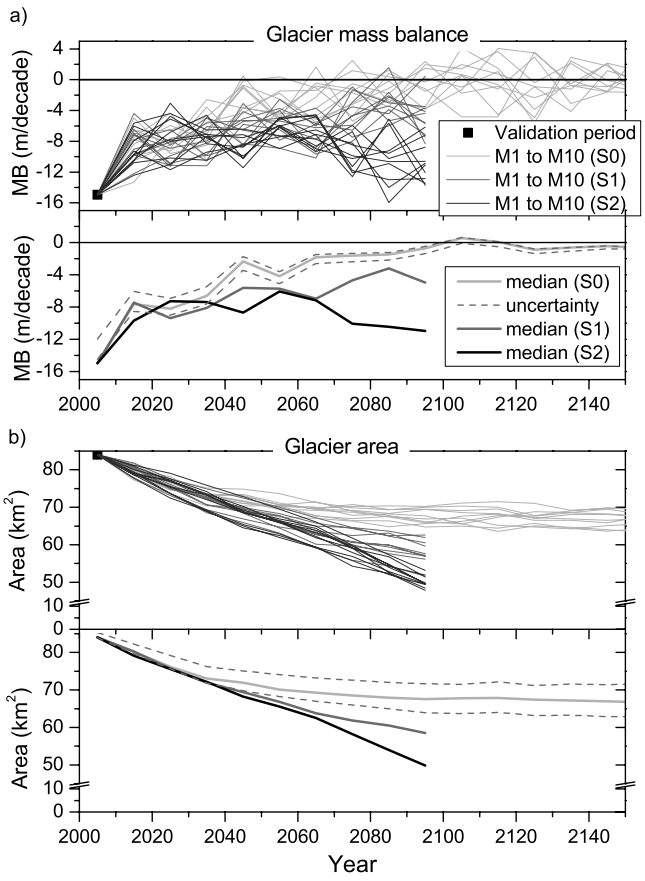

Figure 6. Development of (a) simulated decadal glacier mass balance and (b) glacier area: all scenario members (upper panel) and median for each scenario (lower panel). The dashed lines around the medians for S0 represent the effects of uncertainty in the melt parameters.

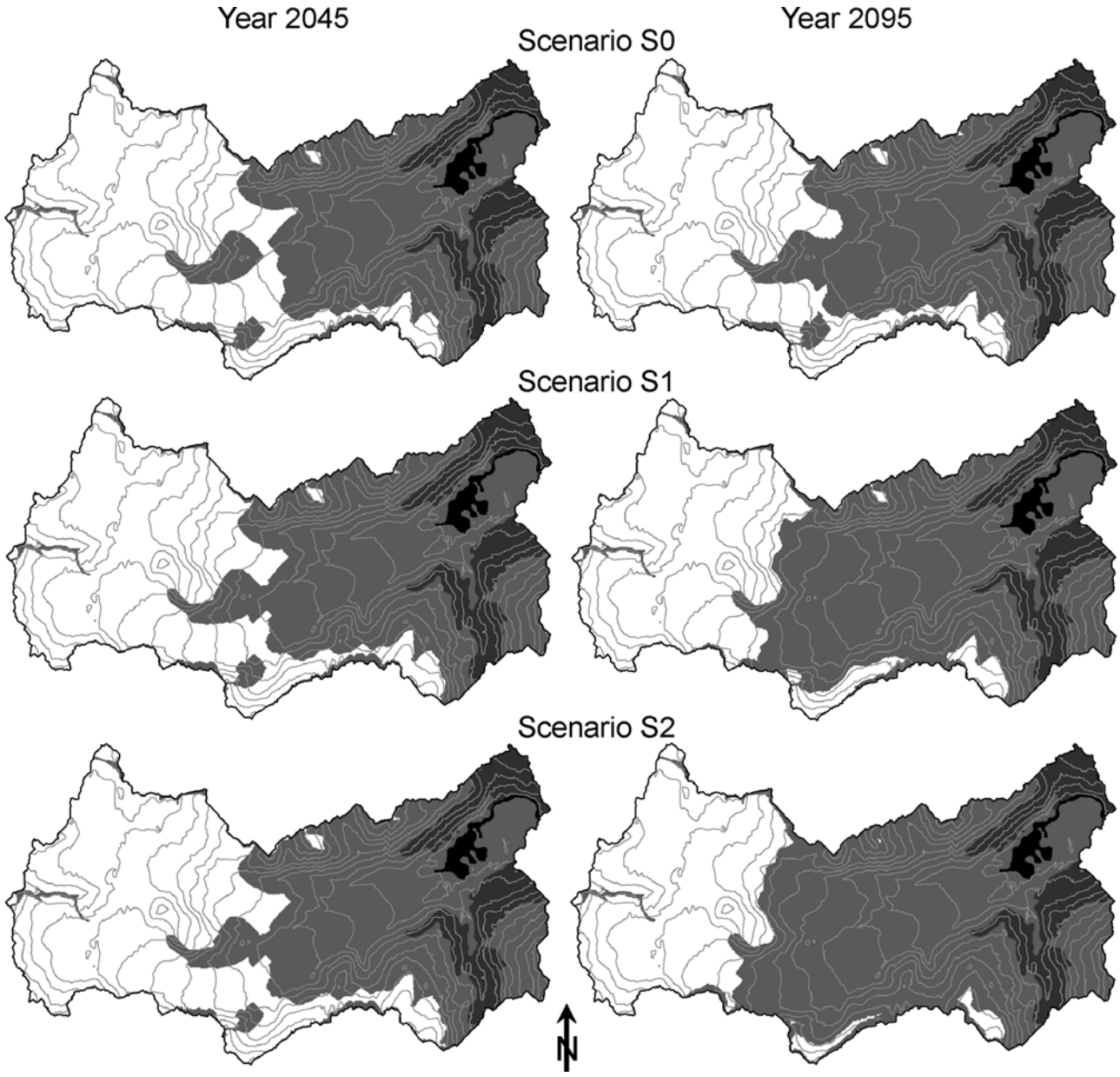

Figure 7. Glacier coverage in the Bridge River basin in 2045 and 2095 under different climate scenarios (Legend as in Figure 4: white: glacier, light grey: non-forest, grey: forest, black: current proglacial lake and river).

[35] Additional sources of error for the calibration period include the land cover from the mid-1990s (i.e. the end of the calibration or beginning of validation period). Glacier extent during the calibration period (1985–1994) may have been somewhat greater, given that glacier retreat likely occurred through that period [*Schiefer et al.*, 2007]. As a result, average August flow was underestimated by ca. 4% for the calibration period and overestimated by ca. 4% in the validation period. Furthermore, mass balance survey data for Bridge Glacier used a slightly different glacier hypsometry and the entire Bridge River basin (and hence the hydrological model) includes additional small glaciers, which may cause some difference in the overall modelled mass balance.

[36] An important source of uncertainty is the use of the temperature-index approach for calculating melt. While the energy balance approach has been implemented in spatially distributed models of catchment hydrology [e.g., *Lehning et al.*, 2006], it is unclear whether it can be applied successfully in regions of complex topography and a low density of (typically valley bottom) stations that record only air temperature and precipitation. This situation describes many glacierized parts of the world, including those in western North America. However, the temperature-index approach has proven to be robust for both hydrological and glaciological simulation over a broad range of geographic conditions, and can provide reasonable results once calibrated, especially for daily to seasonal time scales [*Hock*, 2003]. In

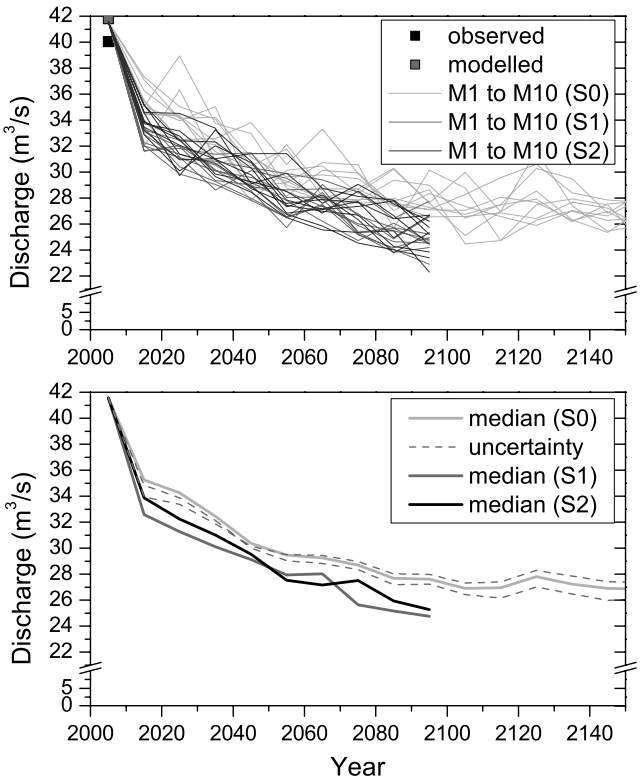

Figure 8. Decadal mean August streamflow: all scenario members (upper panel) and median for each scenario (lower panel). The dashed lines around the medians for S0 represent the effects of uncertainty in the melt parameters.

our study, the use of glacier mass balance information in conjunction with stream hydrographs helped constrain the calibration of the melt factors. Therefore, we are confident that the calibrated model is valid for simulating snow and ice melt under the no-change scenario (S0), which reveals that significant glacier shrinkage will occur. Unfortunately, it is uncertain how the melt factor may vary under changed climatic conditions, introducing uncertainty into the modelled transient glacier and streamflow responses. The stability of melt factors under changing climatic conditions is an important question that deserves further consideration, given the continuing popularity of the temperature index approach in both the hydrological and glaciological communities.

[37] The use of volume-area scaling for modelling glacier changes assumes that there are no lags in response. Glacier dynamics can stall retreat or even maintain advance for some time following an initial shift to negative mass balance. Even discounting dynamic effects, mass loss may initially be dominated by thinning rather than terminal retreat. In this application, Bridge Glacier was already in a state of retreat, suggesting an initial stage of thinning had already occurred. A related issue is that the coefficients in the volume-area scaling relation are not specific to the region, but stem from a dataset of glaciers worldwide [*Chen and Ohmura*, 1990]. However, *Radic et al.* [2007] showed with simulations of hypothetical glaciers that projections are relatively insensitive to the exponent value and are comparable to those from ice flow modelling. They also demonstrated that V-A scaling can produce robust simulations under transient conditions if mass balance-elevation feedback is approximated by removing/adding elevation bands as the glacier retreats/advances (as was done in this study). Nevertheless, the use of V-A scaling to model temporal changes should be tested against observed glacier changes. Subsequent model applications therefore need to verify earlier glacier extents using maps and airphotos and test the sensitivity to the assumed volume-area scaling relation. One source of bias in our approach is that we do not decrease glacier elevations to represent thinning as the glacier retreats. This bias would mean that elevations on the glacier would be biased upward, which would tend to increase accumulation and decrease ablation. The net effect would be to reduce the rate and ultimate amount of retreat.

[38] Additional processes not captured in the current model could influence streamflow in a changing climate. For example, *Braun and Escher-Vetter* [1996] showed that the retreat of firn cover can have a strong influence on glacier runoff in the period following a shift from positive to negative net balance. However, this process may not be so important in the southern Coast Mountains, where signficant firn depletion already appears to have occurred [*Moore and Demuth*, 2001]. In addition, the current model does not represent the effects of vegetation establishment following glacier retreat or other vegetation changes driven by climate change, such as tree establishment at higher elevations. However, these processes are likely to have a second-order effect on streamflow at Bridge River, relative to the effects of glacier retreat.

[39] Despite these issues, the study clearly shows the importance of re-scaling glaciers when assessing the influence of a warming climate on hydrology. The assumption of a continuation of the climate of the past 20 years in S0 was useful for determining the theoretical equilibrium geometry of Bridge Glacier (and hence streamflow from Bridge Basin) under current conditions. As the glacier is in fact far from its equilibrium, it will retreat rapidly within the next few decades and if temperatures further rise the retreat will continue thereafter. As the glaciated area in the basin shrinks rapidly, streamflow reductions for the summer months follow the same pattern. The decrease may only temporarily be slowed during times when temperature increases more strongly as was shown in the second half of the century for S2. Predicted precipitation increases in BC during the winter months are not large enough to offset

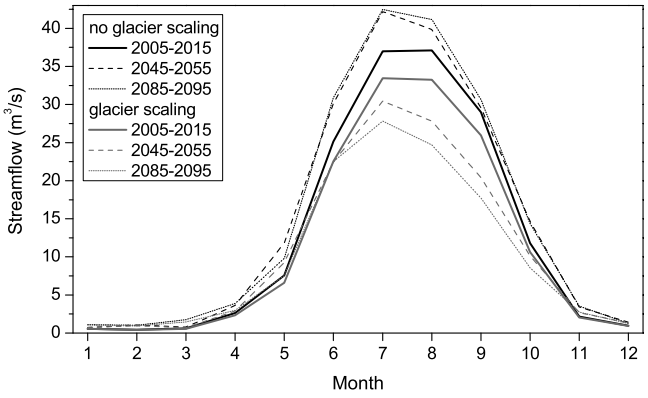

Figure 9. Streamflow response to the first member of S1 (with glacier scaling) and S1a (without glacier scaling).

this development. Some tests with precipitation increases of 5% to 15% added to S0 (not shown), as well as the results from the downscaled scenarios, illustrate this point. This result confirms that glacier retreat appears to be a major cause for the negative streamflow trends in August found across most of BC [*Stahl and Moore*, 2006] and that the period of initial meltwater increase has passed.

[40] The results suggest that climate warming and associated glacier retreat will have significant implications for water resources and aquatic ecology. Glacier-fed rivers are likely to experience a shift from a glacial regime with high flows in mid and late summer, with an associated moderating effect on stream temperature, to a regime that responds to the summer dry period with streamflow recession, low flows and increased temperatures. The simulations, even for the no-change scenario, show that dramatic changes could occur on the time scale of decades, which may be too rapid for some aquatic communities to adapt.

6. Conclusions

[41] In this study we presented a methodology to simulate the transient effects of glacier retreat on streamflow patterns by coupling a semi-distributed hydrological model with a glacier mass balance and glacier scaling model. The volume-area scaling approach has been applied in glaciological studies and is implemented into global climate models, but this appears to be its first application in predictions of future streamflow with a hydrological model. It proved to be a viable approach for generating first-order estimates of coupled glacier and streamflow response to climate change. However, it requires that the model simulates not only streamflow but also glacier mass balance correctly. We showed that, particularly in data sparse areas where climatic gradients are unknown, surveyed mass balances can aid calibration of model parameters and hence greatly reduce the uncertainty in the predictions.

[42] The model results revealed that Bridge Glacier is significantly out of equilibrium with the current climate, and even when a continuation of current climate is assumed, the glacier decreases in area by 20% over the next 50 to 100 years. This retreat is accompanied by a similar decrease in summer streamflow. Under the two warming scenarios, glacier retreat occurred even more rapidly, and the glacier did not appear to approach a new equilibrium after 100 years. These results highlight the need to account for glacier retreat in hydrological simulations, especially for decadal and longer time scales.

Appendix A: The TreeGen Downscaling Algorithm

[43] The TreeGen downscaling algorithm consists of four steps: (1) common principal component analysis (PCA) of observed/GCM predictor fields [*Imbert and Benestad*, 2005]; (2) synoptic map-type classification via a multivariate regression tree [*Cannon et al.*, 2002a, 2002b]; (3) a nonparametric weather generator based on conditional resampling of weather elements from each map-type [*Buishand and Brandsma*, 2001]; and (4) within-type extrapolation based on stepwise linear regression and linear trend analysis [*Imbert and Benestad*, 2005]. Each step is described in turn.

[44] To mitigate potential biases between the NCEP/NCAR Reanalysis and GCM simulated predictors, common PCA was applied to the two datasets [*Imbert and Benestad*, 2005]. First, predictor fields from the reanalysis and GCM were standardized so that the time series for each grid point had zero mean and unit variance during a common 1961–2000 baseline period. Second, standardized data from the reanalysis and the GCM were concatenated to form a single data matrix. Third, PCA was applied to the correlation matrix of the concatenated predictors. Finally, common PC scores from the GCM were rescaled so that their means and variances in the simulated baseline period matched observed values from the same period. To ensure consistency of the simulated seasonal cycle, rescaling was performed on each month separately.

[45] Following the common PCA, synoptic map-types were defined using a multivariate regression tree (MRT) model that recursively split the observed data into groups based on thresholds in the common PC scores [*Cannon et al.*, 2002a, 2002b]. Values of the thresholds were optimized so that the associated daily surface weather elements at the Upper La Joie station were placed into groups (or map-types) that were as homogeneous as possible. Thirteen map-types were selected via cross-validation using the '1-SE' criterion described by *Cannon et al.* [2002a].

[46] Once the synoptic map-types were defined from the historical record, common PC scores from the GCM were then entered into the MRT and each day was classified into one of the map-types. Next, surface weather conditions on a given day were predicted using a nonparametric weather generator based on conditional resampling from cases assigned to that day's map-type [*Buishand and Brandsma*, 2001]. The probability $p(i)$ of randomly selecting weather elements observed on day i as the predicted values on day t was taken to be inversely proportional to the Euclidean distance $d(t-1, i-1)$ between the predicted values on the previous day $t-1$ and historical values of the weather elements on day $i-1$,

$$p(i) = \frac{1/(d(t-1, i-1) + b)^a}{\sum_{h \in I} 1/(d(t-1, h-1) + b)^a},$$

where I is the set of historical days assigned to the predicted map-type occurring on day t and a and b are parameters that modify the shape of the nonparametric probability density function. In this study, values of $a = 7$ and $b = 0.1$ were selected to minimize the absolute bias between predicted and observed lag-1 and lag-2 autocorrelations.

[47] As the nonparametric weather generator sampled cases from the historical dataset, future trends in surface climate conditions were due exclusively to changes in the frequency and timing of the synoptic map-types simulated by the GCM. Additional processing was thus needed to generate values above/below the highest/lowest records in the historical dataset and to accurately reflect trends occurring within map-types. To capture both between- and within-type trends, a modified version of the extrapolation algorithm described by *Imbert and Benestad* [2005] was adopted. For each map-type, multiple linear regression equations linking the common PC scores and the surface weather elements were first created via stepwise regression

based on the Bayesian Information Criterion [*Schwarz*, 1978]. For precipitation, separate models were built for occurrence of precipitation (via regression estimation of event probabilities) and log-transformed precipitation amounts on wet days. Linear trends in predicted temperatures and precipitation amounts relative to baseline from the regression equations were then estimated for each maptype. Finally, these trends were superimposed onto the time series derived from the conditional resampling.

[48] **Acknowledgments.** Financial support from the Government of Canada's Climate Change Impacts and Adaptation Program via Grant A875 is gratefully acknowledged, as is a Natural Sciences and Engineering Research Council (NSERC) Scholarship to JMS, and a NSERC Discovery Grant held by RDM, as well as financial support from the Canadian Foundation for Climate and Atmospheric Science through the Western Canadian Cryospheric Network. BC Hydro kindly provided quality controlled meteorologic data and Mike Demuth supplied the mass balance data. Markus Weiler helped with the implementation of the glacier scaling algorithm into IDL.

References

Bahr, D. B., M. F. Meier, and S. D. Peckham (1997), The physical basis of glacier volume-area scaling, *J. Geophys. Res.*, *102*(B9), 20,355–20,362, doi:10.1029/97JB01696.

Barnett, T. P., J. C. Adam, and D. P. Lettenmaier (2005), Potential impacts of a warming climate on water availability in snow-dominated regions, *Nature*, *438*, 303–309, doi:10.1038/nature0414.

L. N. Braun, and H. Escher-Vetter (1996), Glacial discharge as affected by climate change, *Interpraevent 1996*—Garmisch Partenkirchen, pp. 65–74.

Brown, L. E., D. M. Hannah, and A. M. Milner (2005), Spatial and temporal water column and streambed temperature dynamics within an alpine catchment: Implications for benthic communities, *Hydrol. Processes*, *19*, 1585–1610.

Buishand, T. A., and T. Brandsma (2001), Multisite simulation of daily precipitation and temperature in the Rhine basin by nearest-neighbor resampling, *Water Resour. Res.*, *37*, 2761–2776.

Canadian Hydraulics Centre (2006), *EnSim Hydrologic Reference Manual*, National Research Council, Ottawa, Ontario, 251 pages.

Cannon, A. J., P. H. Whitfield, and E. R. Lord (2002a), Synoptic map-pattern classification using recursive partitioning and principal component analysis, *Mon. Weather Rev.*, *130*(5), 1187–1206.

Cannon, A. J., P. H. Whitfield, and E. R. Lord (2002b), Automated, supervised synoptic map-pattern classification using recursive partitioning trees, In: Preprints, *The 16th Conference on Probability and Statistics in the Atmospheric Sciences*, American Meteorological Society, p. 210–216.

Chen, J., and A. Ohmura (1990), Estimation of alpine glacier water resources and their change since the 1870s, Hydrology in mountainous regions - I. Hydrologic measurements, the water cycle, Proceedings of the two Lausanne Symposia, *IAHS Publ. No*. *193*, 127–135.

Collins, D. N. (2006), Climatic variation and runoff in mountain basins with differing proportions of glacier cover, *Nor. Hydrol.*, *37*(4–5), 315–326.

Dyurgerov, M. (2002), Glacier mass balance and regime: Data of measurements and analysis, Institute of Arctic and Alpine Research, University of Colorado Occasional Paper No. 55.

Fleming, S. W., and G. K. C. Clarke (2003), Glacial control of water resource and related environmental responses to climatic warming: Empirical analysis using historical streamflow data from northwestern Canada, *Can. Water Resour. J.*, *28*, 69–86.

Fountain, A. G., and W. V. Tangborn (1985), The effect of glaciers on streamflow variations, *Water Resour. Res.*, *21*, 579–586.

Hagg, W., L. N. Braun, M. Weber, and M. Becht (2006), Runoff modelling in glacierized Central Asian catchments for present-day and future climate, *Nord. Hydrol.*, *37*, 93–105.

Hamilton, A. S., D. G. Hutchinson, and R. D. Moore (2000), Estimation of winter streamflow using a conceptual streamflow model, *J. Cold Reg. Eng.*, *14*, 158–175.

Hock, R. (2003), Temperature index melt modelling in mountain regions, *J. Hydrol.*, *282*, 104–115, doi:10.1016/S0022-1694(03)00257-9.

Horton, P., B. Schaefli, A. Mezghani, B. Hingray, and A. Musy (2006), Assessment of climate-change impacts on alpine discharge regimes with climate model uncertainty, *Hydrol. Processes*, *20*, 2091–2109, doi:10.1002/hyp.6197.

Imbert, A., and R. E. Benestad (2005), An improvement of analog model strategy for more reliable local climate change scenarios, *Theor. Appl. Climatol.*, *82*, 245–255.

Kalnay, E., et al. (1996), The NCEP/NCAR 40-year Reanalysis Project, *Bull. Am. Meteorol. Soc.*, *77*(3), 437–471.

Koboltschnik, G. R., W. S. Schöner, M. Zappa, and H. Holzmann (2007), Contribution of glacier melt to stream runoff: if the climatically extreme summer of 2003 had happened in 1979, *Ann. Glaciol.*, *46*, 303–308.

Lehning, M., I. Völksch, D. Gustafsson, T. A. Nguyen, M. Stähli, and M. Zappa (2006), ALPINE3D: a detailed model of mountain surface processes and its application to snow hydrology, *Hydrol. Processes*, *10*, 2111–2128.

Lindström, G., B. Johansson, M. Persson, M. Gardelin, and S. Bergström (1997), Development and test of the distributed HBV-96 hydrological model, *J. Hydrol.*, *201*, 272–288.

Mokievsky-Zubok, O., C. S. L. Ommanney, J. Power (1985), NHRI glacier mass balance 1964–1984 (Cordillera and Arctic), Glacier Section, Surface Water Division, National Hydrology Research Institute Internal Report.

Moore, R. D. (1992), Hydrological responses to climatic variations in a glacierized watershed: Inferences from a conceptual streamflow model, in *Using Hydrometric Data to Detect and Monitor Climatic Change*, edited by G. Kite and D. Harvey, National Hydrology Research Institute, Saskatoon, p. 79–88.

Moore, R. D. (1993), Application of a conceptual streamflow model in a glacierized drainage basin, *J. Hydrol.*, *150*, 151–168.

Moore, R. D. (2006), Stream temperature patterns in British Columbia, Canada, based on routine spot measurements, *Can. Water Resour. J.*, *31*, 41–56.

Moore, R. D., and M. N. Demuth (2001), Mass balance and streamflow variability at Place Glacier, Canada, in relation to recent climate fluctuations, *Hydrol. Processes*, *15*(18), 3473–3486.

Mote, P., E. Salathe, and C. Peacock (2005), Scenarios of future climate for the Pacific Northwest, report, Climate Impacts Group, University of Washington. (http://www.cses.washington.edu/db/pdf/kc05scenarios462.pdf)

Nash, J. E., and J. V. Sutcliffe (1970), River flow forecasting through conceptional models, Part I: A discussion of principles, *J. Hyrol.*, *10*, 282–290.

Oerlemans, J. (2005), Extracting a climate signal from 169 glacier records, *Science*, *308*(5722), 675–677, doi:10.1126/science.1107046.

Oerlemans, J., B. Anderson, A. Hubbard, Ph. Huybrechts, T. Johannesson, W. H. Knap, M. Schmeits, A. P. Stroeven, R. S. W. van de Wal, J. Wallinga, and Z. Zuo (1998), Modelling the response of glaciers to climate warming, *Clim. Dyn.*, *14*, 267–274.

Østrem, G., and M. M. Brugman (1991), *Glacier Mass-Balance Measurements: A manual for field and office work*, National Hydrology Research Institute Science Report No. 4, Minister of Suppy and Services, Ottawa.

Radic, V., and R. Hock (2006), Modeling future glacier mass balance and volume changes using ERA-40 reanalysis and climate models; A sensitivity study at Storglaciären, Sweden, *J. Geophys. Res.*, *111*, F03003, doi:10.1029/2005JF000440.

Radic, V., R. Hock, and J. Oerlemans (2007), Volume-area scaling vs flowline modelling in glacier volume projections, *Ann. Glaciol.*, *46*, 234–240.

Rees, H. G., and D. N. Collins (2006), Regional differences in response of flow in glacier-fed Himalayan rivers to climatic warming, *Hydrol. Processes*, *20*, 2157–2169, doi:0.1002/hyp.6209.

Schaefli, B., and H. V. Gupta (2007), Do Nash values have value?, *Hydrol. Processes*, doi:10.1002/hyp.6825.

Schaefli, B., B. Hingray, M. Niggli, and A. Musy (2005), A conceptual glacio-hydrological model for high mountainous catchments, *Hydrol. Earth Syst. Sci.*, *9*, 95–109.

Schiefer, E., B. Menounos, and R. Wheate (2007), Recent volume loss of British Columbian glaciers, Canada, *Geophys. Res. Lett.*, *34*, L16503, doi:10.1029/2007GL030780.

Schwarz, G. (1978), Estimating the dimension of a model, *Ann. Stat.*, *6*(2), 461–464.

Semenov, M. A., R. J. Brooks, E. M. Barrow, and C. W. Richardson (1998), Comparison of the WGEN and LARS-WG stochastic weather generators in diverse climates, *Clim. Res.*, *10*, 95–107.

Singh, P., and L. Bengtsson (2005), Impact of warmer climate on melt and evaporation for the rainfed, snowfed and glacierfed basins in the Himalayan region, *J. Hydrol.*, *300*, 140–154.

Singh, P., and N. Kumar (1997), Impact assessment of climate change on the hydrological response of a snow and glacier melt runoff-dominated Himalayan river, *J. Hydrol.*, *193*, 316–350.

Stahl, K., and R. D. Moore (2006), Influence of watershed glacier coverage on summer streamflow in British Columbia, Canada, *Water Resour. Res.*, *42*, W06201, doi:10.1029/2006WR005022.

Van de Wal, R. S. W., and M. Wild (2001), Modelling the response of glaciers to climate change by applying volume-area scaling in combination with a high resolution GCM, *Clim. Dyn.*, *18*, 359–366, doi:10.1007/s003820100184.

WWF (2005), *An overview of glaciers, glacier retreat, and subsequent impacts in Nepal, India and China*, World Wildlife Fund, Nepal Program.

Zappa, M., and C. Kan (2007), Extreme heat and runoff extremes in the Swiss Alps, *Nat. Hazards Earth Syst. Sci.*, *7*, 375–389.

A. J. Cannon and D. Hutchinson, Environment Canada, 201-401 Burrard Street, Vancouver, BC V6C 3S5, Canada.

R. D. Moore and J. M. Shea, Department of Geography, The University of British Columbia, 1984 West Mall, Vancouver, B.C. V6T 1Z2, Canada.

K. Stahl, Department of Geosciences, University of Oslo, Oslo, Norway. (kerstin.stahl@geo.uio.no)